Applied Geochemistry 100 (2019) 42–54

Contents lists available at ScienceDirect

Applied Geochemistry

journal homepage: www.elsevier.com/locate/apgeochem

Sodium transport and attenuation in soil cover materials for oil sands mine reclamation

Colton J. Vessey[a], Matthew B.J. Lindsay[a,*], S. Lee Barbour[b]

[a] Department of Geological Sciences, University of Saskatchewan, Saskatoon, SK, S7N 5E2, Canada
[b] Department of Civil, Geological and Environmental Engineering, University of Saskatchewan, Saskatoon, SK, S7N 5A9, Canada

ARTICLE INFO

Keywords:
Oil sands
Reclamation
Soil covers
Geochemistry
Sodium

ABSTRACT

Reclamation soil covers are used in oil sands mine closure to support vegetative growth over tailings. Geochemical processes within these covers may impact solute transport during upward migration of oil sands process-affected water (OSPW) from the underlying tailings. In this study, we examined the geochemical processes controlling Na transport and attenuation within the peat and clay-till cover soils at Sandhill Fen in northern Alberta, Canada. We analyzed soil core samples collected along transects of this 54-ha pilot-scale oil sands mine reclamation wetland. The geochemical (Na, Ca, Mg, K, Cl, SO_4, HCO_3) and isotopic (δ^2H, $\delta^{18}O$) compositions of extracted pore water were analyzed statistically to identify OSPW and fresh surface water within the cover. Depth-dependent trends in pore water sodium concentrations were not apparent, suggesting that the soil cover had been fully flushed by a mixture of OSPW and fresh surface water used to flood the fen. Relative concentrations of Na, Ca and Mg were used to define the extent of cation exchange within the clay cover. Complementary laboratory column experiments showed that cation exchange removed up to 50% of dissolved Na as the first pore volume of simulated OSPW passed through the peat and till. However, Na attenuation by these materials declined rapidly and was limited after 4 (peat) to 7 (till) pore volumes of OSPW flushing. Reactive transport modeling confirmed that cation exchange was the dominant control on Na attenuation and corresponding Ca and Mg release within the till and peat columns. Mineral precipitation-dissolution reactions also influenced dissolved Ca and Mg concentrations and, therefore, indirectly impacted Na attenuation. Overall, this study helps constrain the geochemical processes controlling Na transport and attenuation in oil sands reclamation soil covers exposed to OSPW, and indicates that the attenuation of Na from OSPW by these covers is short-lived.

1. Introduction

Surface mining operations have disturbed large land areas in the Athabasca Oil Sands Region (AOSR) of northern Alberta, Canada. The mine site footprint in this region currently exceeds 900 km^2, which corresponds to approximately 20% of the estimated 4800 km^2 surface mineable area (Government of Alberta, 2017). Mining companies are required to reclaim post-mining landscapes to an equivalent land capacity; however, reclamation on this scale presents considerable challenges and is unprecedented globally (Gosselin et al., 2010).

Peatlands comprise over 50% of the Western Boreal Plains (WBP) region and are a keystone ecosystem for water retention and regulation (Ferone and Devito, 2004; Vitt et al., 1996). Fen reclamation was initially deemed unachievable as natural fens form over millennia (Clymo, 1983); however, two pilot-scale reclamation fens have been constructed to date: the Nikanotee Fen at the Millennium mine lease (Kessel et al., 2018; Ketcheson et al., 2017; Scarlett et al., 2017; Simhayov et al., 2017); and the Sandhill Fen at the Mildred Lake mine lease (Bradford et al., 2017; Nicholls et al., 2016; Oswald and Carey, 2016; Reid and Warren, 2016; Vitt et al., 2016). These constructed fens are designed to ensure that the constructed landscape will provide sufficient freshwater to sustain the fen (Price et al., 2010).

Oil sands reclamation landscapes may contain tailings or other materials generated during bitumen mining, extraction, or upgrading. Oil sands process-affected water (OSPW) generally dominates pore water chemistry within fluid fine tailings (FFT) and coarse tailings sand. This water is characterized by elevated concentrations of dissolved salts, naphthenic acids, petroleum hydrocarbons and trace elements (Allen, 2008; Apostol et al., 2004; Ketcheson et al., 2016; Pouliot et al., 2012). Major ions in tailings pore water include Na, Cl, HCO_3 and SO_4

* Corresponding author.
E-mail address: matt.lindsay@usask.ca (M.B.J. Lindsay).

https://doi.org/10.1016/j.apgeochem.2018.10.023
Received 30 July 2018; Received in revised form 27 September 2018; Accepted 29 October 2018
Available online 03 November 2018
0883-2927/

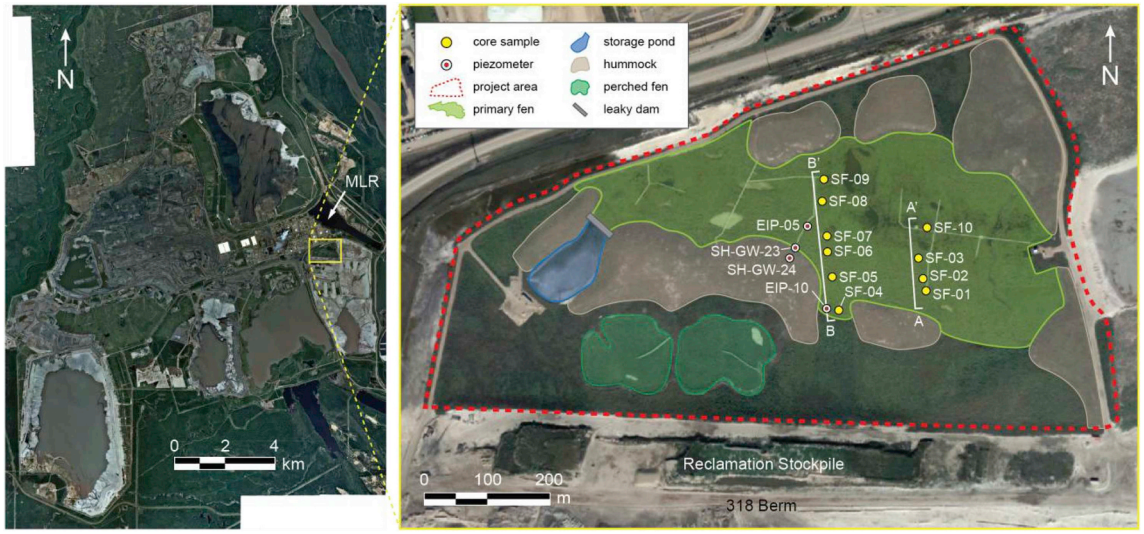

Fig. 1. Composite air photo showing the Mildred Lake lease (left) and the study site location. Satellite image showing enlarged view of Sandhill Fen (right) with landform features, selected piezometer locations, and soil sampling locations along transects A –A′ and B – B'. Satellite image attributed to Google™ Earth © 2018 Digital Globe.

derived from the ore extraction process and connate water from the bitumen ore (Allen, 2008; Chalaturnyk et al., 2002). Mixing FFT with coarse tailings sand and gypsum [$CaSO_4{\cdot}2H_2O$] to produce composite tailings (CT) can enhance settlement and dewatering (MacKinnon et al., 2001; Matthews et al., 2002; Kasperski and Mikula, 2011). Pore water within CT deposits is derived from OSPW and is, therefore, characterized by high electrical conductivity, elevated Na concentrations (900–1200 mg L^{-1}), and enriched $\delta^{18}O$ (−11‰) and $\delta^{2}H$ (−115‰) values (MacKinnon et al., 2001; Allen et al., 2008; Baer et al., 2016; Dompierre et al., 2016). Gypsum addition directly increases dissolved Ca and SO_4 concentrations, whereas elevated Na results from ion exchange reactions at FFT clay-mineral surfaces.

Self-weight consolidation, surcharge loading as well as natural topographic gradients result in discharge of CT pore water to surface with the concomitant advective-dispersive transport of OSPW into overlying reclamation materials (Cilia, 2017; Dompierre et al., 2017; Rezanezhad et al., 2012a). Elevated sodium concentrations in reclamation covers increase plant water stress and, at high concentrations, may become toxic to some terrestrial and aquatic organisms (Apostol et al., 2004; Ketcheson et al., 2016; Pouliot et al., 2012; Rezanezhad et al., 2012b; Kessler et al., 2010). Although some vegetation used in oil sands mine reclamation can tolerate elevated Na concentrations (Rezanezhad et al., 2012b), high concentrations may lead to reduced biomass or plant performance (Glaeser et al., 2016).

Clay-rich glacial tills and peat material are commonly salvaged to use in reclamation at oil sands mines, including in constructed wetlands. Cation exchange reactions within these types of soils can limit Na transport (Kessler et al., 2010; McCarter et al., 2018). In the case of constructed fens, this attenuation mechanism could reduce the ecological impacts of OSPW for an initial time period. Previous studies on OSPW have demonstrated that Na^+ exchange for Ca^{2+} and Mg^{2+} in clay-rich surficial sediments from the AOSR can promote Na attenuation (Holden et al., 2011, 2013; Abolfazlzadehdoshanbehbazari et al., 2013). Rezanezhad et al. (2012b) reported substantial Na attenuation during OSPW transport through peat *via* sorption and diffusion into immobile pores. Although these studies indicate that cation exchange reactions within reclamation soil cover materials promote Na attenuation, the long-term influence of this process on water chemistry remains poorly constrained.

The cation exchange sites of the salvaged peat and glacial soils are initially dominated by Ca^{2+} and Mg^{2+} (Holden et al., 2011, 2012; 2013; NorthWind Land Resources, 2014). However, sustained OSPW migration will result in declining Na attenuation over time as exchange sites become Na^+ dominated. Cation exchange within the reclamation soil cover materials can be described by the following mass action reactions:

$$2Na^+ + CaX_2 \rightleftharpoons 2NaX + Ca^{2+} \quad (1)$$

$$2Na^+ + MgX_2 \rightleftharpoons 2NaX + Mg^{2+} \quad (2)$$

where *X* represents a cation exchange site. Increasing pore water Ca and Mg concentrations may, therefore, serve as an early indication of OSPW migration through these cover materials. Declining Na attenuation may have important implications for water quality, but also the physical properties and hydrologic performance of reclamation soil covers (Kessler et al., 2010; Qadir and Schubert, 2002; Rezanezhad et al., 2012a). For example, when Na concentrations are high relative to other dissolved salts, clay-particle dispersion can deteriorate soil structure, leading to decreased hydraulic conductivity, infiltration capacity and plant-available water (Curtin and Naidu, 1998; Qadir and Schubert, 2002; Rengasamy and Sumner, 1998; Suarez et al., 1984).

This study examined the capacity of reclamation soils used within a constructed fen to mitigate Na transport. Field samples were collected to examine the extent of Na transport and attenuation within a pilot-scale oil sands constructed fen. Subsequent laboratory experiments were conducted to assess the sodium attenuation processes and the cation exchange capacity of the individual soil types (i.e. clay-rich glacial till, salvaged peat and processed tailings sand). This study focuses on the geochemical process impacting sodium transport through soil reclamation materials. The results will inform future designs of reclamation landscapes which may be exposed to saline groundwater or OSPW and improve our ability to manage future water quality at oil sands mines.

2. Materials and methods

2.1. Field investigation

2.1.1. Study site

Sandhill Fen is located approximately 40 km north of Fort McMurray, Alberta (57.057°N, 111.600°W) at the Mildred Lake mine lease (Fig. 1). This 54-ha pilot-scale wetland was constructed in 2012 over a decommissioned open pit containing approximately 40 m of interbedded composite tailings (CT) and tailings sand.

Sandhill Fen contains a 15-ha primary fen area, plus two perched fens and a storage pond. Within the primary fen, the CT deposit is overlain by

10 m of processed tailings sand and capped with a 1-m thick reclamation soil cover comprised of live peat materials overlying clay-rich Pleistocene till salvaged and stockpiled during mining. Approximately 0.5 m of peat overlies 0.5 m of clay-rich Pleistocene till within the primary fen, except for a few locations where only till was placed. An underdrainage network installed within the tailings sand provided an initial operational control on the upward migration of OSPW from the underlying CT deposit; however, the underdrainage system was shut off in 2014 prior to the field sampling undertake for this study in 2015. Additional details on the construction of Sandhill Fen, which was completed in December 2012, are provided by Reid and Warren (2016).

Processed tailings sand and Pleistocene fluvial sand was also used during construction of a series of sand hummocks adjacent to the fen (Fig. 1). These hummocks were designed to direct freshwater recharge and the associated groundwater flow to the fen. Surface water from a storage pond slowly feeds into the primary fen, which then flows eastward toward a discharge point. Hydrogeological monitoring and modeling identified that in addition to settlement induced pore-water release, vertical upwelling of OSPW was also occurring due to recharge into a large tailings sand dyke immediately south of the fen. This recharge resulted in upward hydraulic gradients that caused upward vertical transport of pore water from underlying tailings sand and CT through the south and south-eastern flanks of the fen (BGC, 2015). Water levels measured in selected piezometer nests adjacent to transect B – B' revealed upward hydraulic gradients below the reclamation soil cover (Figure S1). Active water management which included the addition of freshwater to the fen and operation of the underdrainage network to control the water table elevation within the tailings sand layer below the primary fen was only in operation until early 2014.

2.1.2. Soil sampling

Core samples of the reclamation soil cover were collected in July 2015 from 10 locations along two south to north trending transects across Sandhill Fen (Fig. 1). These transects, A – A′ and B – B′ were selected based upon results of hydrogeological modeling (BGC, 2015) to capture locations where upward vertical groundwater migration was expected. Foot access was limited along transect A – A' and sample locations were sporadic, and therefore, not analyzed for pore water chemistry. Samples were collected into clean polyvinyl chloride (PVC) liners using a soil core sampler that was advanced using a slide hammer. Sequential cores were collected over 0.15 m intervals a maximum depth of 0.9 m, which approached the lower boundary of the reclamation soil cover. Upon retrieval, the core tubes were immediately capped and sealed, refrigerated (4 °C), and transported to the University of Saskatchewan for analysis.

2.1.3. Pore water extraction

Pore water was extracted from 38 soil samples collected at six locations (SF-04, SF-05, SF-06, SF-07, SF-08, and SF-09) along transect B – B'. Pore water was extracted utilizing a modified version of the method described by Moncur et al. (2013). Briefly, sub-samples of each core were packed into clean stainless-steel cylinders between a porous stainless-steel plate (bottom) and piston (top). Viton O-rings ensured a water-tight seal between the piston and cylinder wall. Acid-washed Viton tubing was connected to an outlet at the bottom of the cylinder to facilitate sample collection. A hydraulic press was used to advance the piston and compress the sample; extracted water was collected into polypropylene (PP) syringes (Norm-Ject, Henke-Sass Wolf GmbH, Germany) connected to the outlet tubing with a polycarbonate Luer-Lock valve.

2.2. Laboratory columns

2.2.1. Experimental setup

Laboratory column experiments inlcuded the three principal soil cover materials used during construction of the Sandhill Fen: (i) clay-rich Pleistocene till; (ii) salvaged/stockpiled live peat; and (iii) Pleistocene fluvial sand. Each material was packed into two separate acrylic columns (Soil Measurement Systems, USA) measuring 10 cm long with a 7.6 cm internal diameter. The columns contained an 8-cm long interval of reclamation material positioned between two 1-cm layers of acid-washed #20–#40 mesh Ottawa sand. Packing was performed to ensure bulk density was consistent with field samples and among both columns for each material. A pre-determined mass was packed in 1 cm length intervals to achieve desired densities. Each column was fitted with one inlet and one outlet port. The inlet port was connected to a high-precision, low-flow multi-channel peristaltic pump (Model 2058, Watson-Marlow, Inc.) using polytetrafluoroethylene (PTFE) tubing. The outlet port was connected in series to a sealed overflow sampling cell and then an overflow waste jug. The columns were wrapped in aluminum foil to limit light exposure and, therefore, inhibit phototrophic growth and minimize photochemical reactions. Before starting the experiment, the columns were first flushed for 48 h with $CO_{2(g)}$, which is highly soluble in water and, therefore, minimizes bubble entrapment during initial water saturation.

Two input solutions were prepared to simulate groundwater chemistry observed in monitoring wells located below the reclamation cover at Sandhill Fen. The chemistry for Input 1 and 2 (Table 1) solutions were based upon 2013 groundwater chemistry data from wells SH-GW-23-D and EIP-10-D (2.3 m below ground surface; Fig. 1), respectively (BGC, 2015). These solutions were prepared by dissolving ACS reagent-grade salts (i.e., Na_2SO_4, NaCl, $NaHCO_3$, $CaCl_2{\cdot}2H_2O$, $MgCl_2{\cdot}6H_2O$, KCl) into deionized (DI) water. These solutions were stored in amber-glass bottles and pumped into the columns in an upward direction to avoid gravity drainage. All glassware was cleaned with 10% (v/v) hydrochloric acid thoroughly rinsed with DI water before use.

2.2.2. Water sampling

Column influent and effluent samples were collected weekly to monitor ion exchange reactions over time. The influent samples were collected directly from the stock solution, while effluent samples were collected from the sampling cell. Samples were collected into PP syringes and either transferred directly into glass culture tubes or passed through 0.45 μm PES syringe filters.

2.3. Sample analysis

2.3.1. Solids analysis

Gravimetric water contents of field samples and column materials were determined in triplicate by weighing before and after oven drying at 105 °C for at least 24 h. Cation exchange capacity was measured using a modified methylene blue method (Holden et al., 2012) in which 20 g equivalent dry weight of each sample was dispersed in 500 mL of deionized water (DI) and then titrated using a 0.02 M methylene blue solution. The titration endpoint corresponded to the volume of methylene blue solution required to produce a blue halo around sample suspensions pipetted onto filter paper. Final CEC values were calculated using the formula reported by Holden et al. (2012). The CEC determinations were performed in triplicate for two samples to assess reproducibility.

Table 1
Target input solution chemistry for column experiments.

Parameter	Units	Input 1	Input 2
pH		8.5	8.5
sodium (Na)	mg L^{-1}	1000	1000
magnesium (Mg)	mg L^{-1}	16	7
potassium (K)	mg L^{-1}	18	18
calcium (Ca)	mg L^{-1}	3	3
bicarbonate (HCO_3)	mg L^{-1}	1100	1100
chloride (Cl)	mg L^{-1}	650	900
sulfate (SO_4)	mg L^{-1}	900	100

X-ray diffraction (XRD) was performed with a Co Kα1 source (1.78901 Å), and a Fe K-β filter at 45 mA and 40 kV. Air-dried samples were lightly ground in an agate mortar and pestle and mounted on glass slides (Moore and Reynolds, 1999). The XRD instrument (Empyrean, PANalytical) was operated using a 3–80° 2θ step size and 50-min counting. Phase identification was performed with Match! (v. 2.3.3), using the Crystallography Open Database (Gražulis et al., 2009).

2.3.2. Water analyses

Measurements of pH, electrical conductivity (EC) and alkalinity were made immediately following pore water extraction or column sampling. The pH electrode (Orion 9678BNWP, Thermo Scientific, USA) was calibrated to NIST-traceable pH 4, 7 and 10 buffers. The conductivity cell (Orion 013010MD, Thermo Scientific, USA) was calibrated to NIST-traceable conductivity standards. Calibrations were checked before each measurement and recalibration was performed as required. The remaining sample was passed through 0.2 µm polyethersulfone (PES) filter membranes. Alkalinity was determined by titration with 1.6 N H_2SO_4 to the bromocresol green methyl red endpoint (i.e., 4.5). Samples were collected into high-density polyethylene (HDPE) bottles, preserved according to standard methods, and stored at 4 °C until chemical analysis. Inorganic anion concentrations were determined by ion chromatography (IC). Major element concentrations were determined by inductively coupled plasma – optical emission spectroscopy (ICP-OES) for samples acidified to pH < 2 using trace-metal grade nitric acid. For pore water extracted from the field samples, stable isotopes of water (δ^2H-H_2O, δ^{18}O-H_2O) were measured using a vapor equilibration method (Wassenaar et al., 2008) by cavity ring down spectroscopy (CRDS).

2.4. Data analysis

Statistical methods, thermodynamic equilibrium modeling, and reactive transport modeling were used to support data interpretation. Principal component analysis (PCA) and Pearson correlations was performed in ioGas software (v. 6.3.1) to examine relationships between soil pore water constituents. These data were treated using the centered log ratio transformation prior to statistical analysis.

Thermodynamic equilibrium modeling of soil pore water and column influent and effluent samples was performed using the PHREEQCi (Version 3.1.5) code (Parkhurst and Appelo, 2013) with the WATEQ4F database (Ball and Nordstrom, 1991). Modelled saturation indices (SIs) for relevant mineral phases was used to assist with data interpretation. Data quality for all water analyses was assessed using speciated charge balance errors (CBE's) calculated using PHREEQCi. Samples were re-analyzed by ICP-OES and IC when CBE's exceeded ± 5%.

One-dimensional reactive transport modeling of the column experiments was also performed using PHREEQCi. Models were developed to simulate cation exchange, precipitation-dissolution and biogeochemical reactions within each column and, therefore, to improve understanding of controls on element transport through reclamation soil materials. Details on model parameterization, optimization and results are discussed below.

3. Results and discussion

3.1. Field investigation

3.1.1. Physical characteristics

Gravimetric water contents ranged from 17 to 85% (w/w), but were consistently lower within the till relative to the peat layer. The water content of the till samples averaged 23 ± 4.0% (w/w) and 69 ± 19% (w/w) for the peat samples. The till samples were assumed to be at saturation. For example, for an average particle density of 2.7 g cm^{-3} a water content of 23% the porosity of a saturated sample would be approximately 0.38. Measured CEC values for the till samples ranged from 5.9 to 14.1 meq 100 g^{-1} with an average value for all samples (n = 16) of 9.3 ± 2.4 meq 100 g^{-1} (Table S1). Samples from locations SF-06 (18–24 cm) and SF-07 (18–24 cm) were analyzed in triplicate and results were highly reproducible at 10.8 ± 1.3 meq 100 g^{-1} and 8.0 ± 1.6 meq 100 g^{-1}, respectively. These values are slightly higher than methylene blue CEC values previously reported for Pleistocene till in the region (Holden et al., 2012). Methylene blue titrations were attempted for the peat samples; however, visual determination of the titration endpoint was challenging and calculated CEC values were not reproducible. Mineralogical analysis of the till samples revealed that the clay fraction was dominated by kaolinite, illite and chlorite (Figure S2). The measured CEC values are generally consistent with the clay mineralogy and content of these samples (Carroll, 1959; Holden et al., 2012).

3.1.2. Pore water chemistry

Pore water pH ranged from 5.6 to 8.3 (average 7.0 ± 0.7) with values less than 7.0 limited to the peat layer (Fig. 2a). The lowest pH values were observed in uppermost sample from locations SF-04 and SF-05. Alkalinity exhibited a wide range from 43 to 610 mg L^{-1} (as $CaCO_3$) among all samples. These values generally increased with depth at locations SF-04, SF-05, SF-08, and SF-09. An opposite trend was observed at SF-07, which was located within a till zone with no overlying peat layer (i.e., till extending from surface to 1.0 m depth). Alkalinity averaged 270 ± 150 mg L^{-1} (as $CaCO_3$) among all sites, yet there was generally no consistent trend with depth or location along the transect. The lowest measured alkalinity values, which were less than 60 mg L^{-1} as $CaCO_3$, occurred at depths where pore water pH was below 6.0. For samples with pH greater than 6.4, HCO_3^- is the dominant contributor to alkalinity. Electrical conductivity averaged 2200 ± 800 µS cm^{-1} and generally decreased from location SF-04 to SF-08. Elevated EC values of up to 4000 µS cm^{-1} observed in the uppermost sample at locations SF-04, SF-05 and SF-07 were attributed to evaporation (Fig. 2a).

In general, pore water Cl concentrations followed a similar spatial trend to EC values. Concentrations ranged from 28 to 880 mg L^{-1} (average 220 ± 230 mg L^{-1}) with the highest concentrations observed in the uppermost samples from locations SF-04 and SF-05 (Figure S3). Average Cl concentrations for individual locations generally decreased from location SF-04 (680 ± 110 mg L^{-1}) to SF-08 (64 ± 5.6 mg L^{-1}). Despite similar spatial trends, Cl concentrations and EC values were poorly correlated, suggesting EC is derived from different ions at different sampling locations or depths. Dissolved SO_4 concentrations generally exhibited an opposite spatial trend to that of Cl. Sulfate concentrations ranged from 260 to 2200 mg L^{-1} (average 830 ± 410 mg L^{-1}) among all sites, with the highest average concentration found at SF-07 (1140 ± 530 mg L^{-1}). Consistent with EC, concentrations of both Cl and SO_4 exhibited increases near surface at locations SF-04, SF-05 and SF-07.

Pore water Ca concentrations (Figure S3) averaged 250 ± 110 mg L^{-1} among all samples; however, these concentrations were much lower at SF-04 (140 ± 78 mg L^{-1}) compared to SF-06 (360 ± 46 mg L^{-1}) and SF-07 (360 ± 130 mg L^{-1}). Corresponding Mg concentrations followed similar spatial trends and averaged 65 ± 34 mg L^{-1} overall. In contrast, average pore water Na concentrations were more than five times higher at SF-04 (560 ± 30 mg L^{-1}) than at SF-07 (100 ± 50 mg L^{-1}) or SF-08 (88 ± 11 mg L^{-1}). These Na concentrations exhibited a similar spatial trend to that of Cl, where the highest average values were also observed at SF-04. Sodium adsorption ratio (SAR) supports the Na and Cl data with the highest values at SF-04 (11.63 ± 2.6 meq L^{-1}) and decreases towards the primary fen at location SF-09 (1.65 ± 0.15 meq L^{-1}) (Fig. 2b). These trends are generally opposite to observed trends in Ca, Mg and SO_4, indicating that soil pore water within Sandhill Fen is derived from more than one source.

Statistical analyses revealed positive relationships between several parameters including: (i) Na and Cl; (ii) Mg, Ca and SO_4; and (iii) K and HCO_3 (Figure S4). The PCA results revealed a strong negative correlation on the PC3 axis between K and HCO_3. On the PC1 axis there was a well-defined opposing relationship between Ca, Mg and SO_4 versus Na

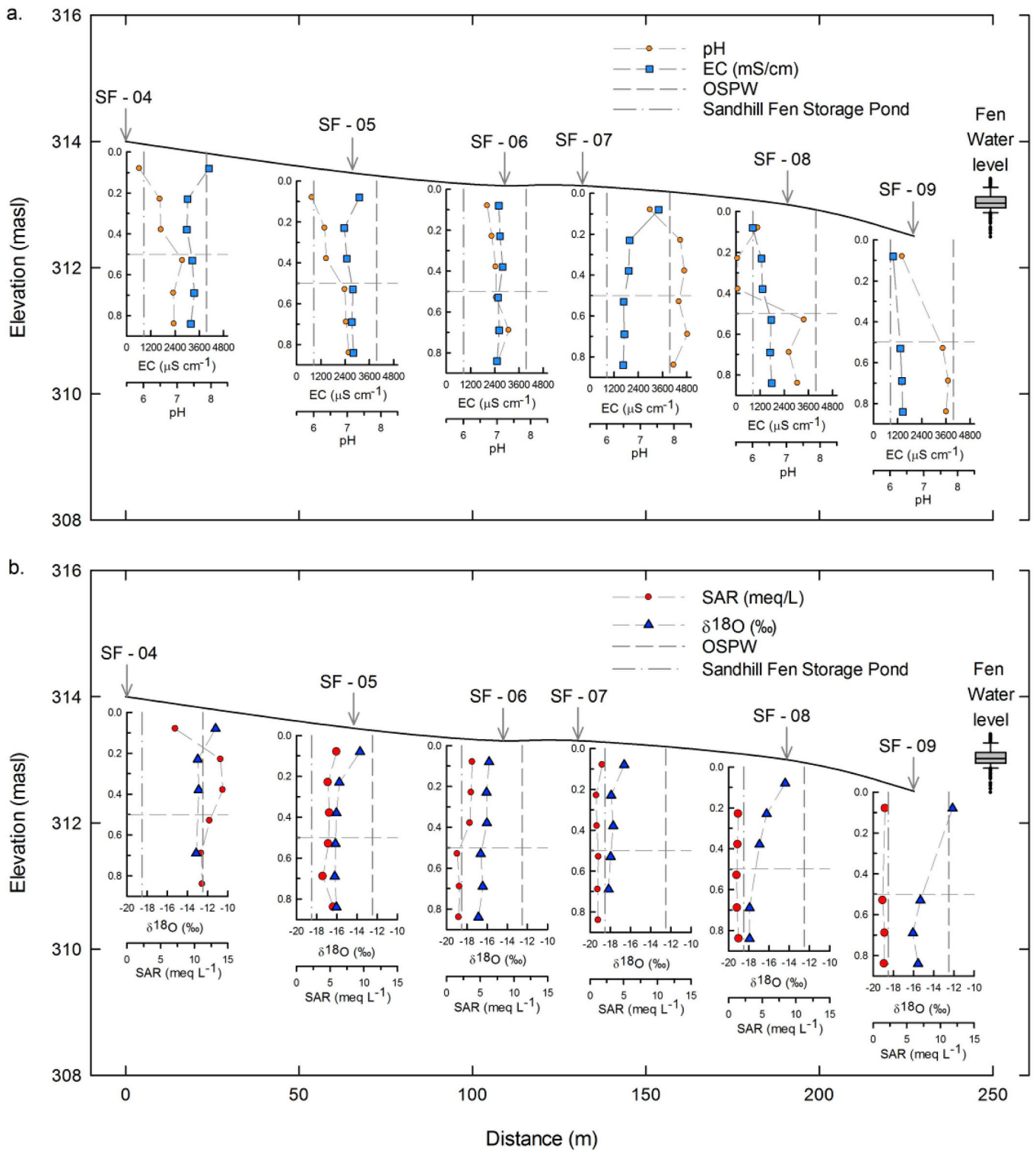

Fig. 2. Surface topography (solid black line) along transect B – B′, soil pore water samples plotted with depth (meters below surface) displaying pH, and EC (a.), and SAR, and $\delta^{18}O$ (b.). Horizontal dashed line denotes approximate interface between sub-soil and peat at all locations except SF-07. Vertical dashed lines correspond to EC (a.) and $\delta^{18}O$ (‰) (b.) mixing end member values from OSPW and the Sandhill Fen storage pond. Water level box plot data was collected from ponded water within the primary fen (BGC, 2015).

and Cl. These statistical trends are consistent with special variation within the geochemical data along the sampling transect.

The composition of field pore water samples was compared to two end members (Fig. 2): a OSPW pore water collected from a well screened within the saline CT deposit (EIP-10-D) (BGC, 2015); and a 2012 surface water samples from the Mildred Lake Reservoir (MLR) and the Sandhill Fen storage pond (SF-SP), both representing a fresh water end member. The resulting Piper diagram (Fig. 3) revealed a mixing trend between Na-Cl type water to Ca-Mg-SO_4 type water. The Na-Cl type water composition is generally consistent with OSPW (Fig. 1),

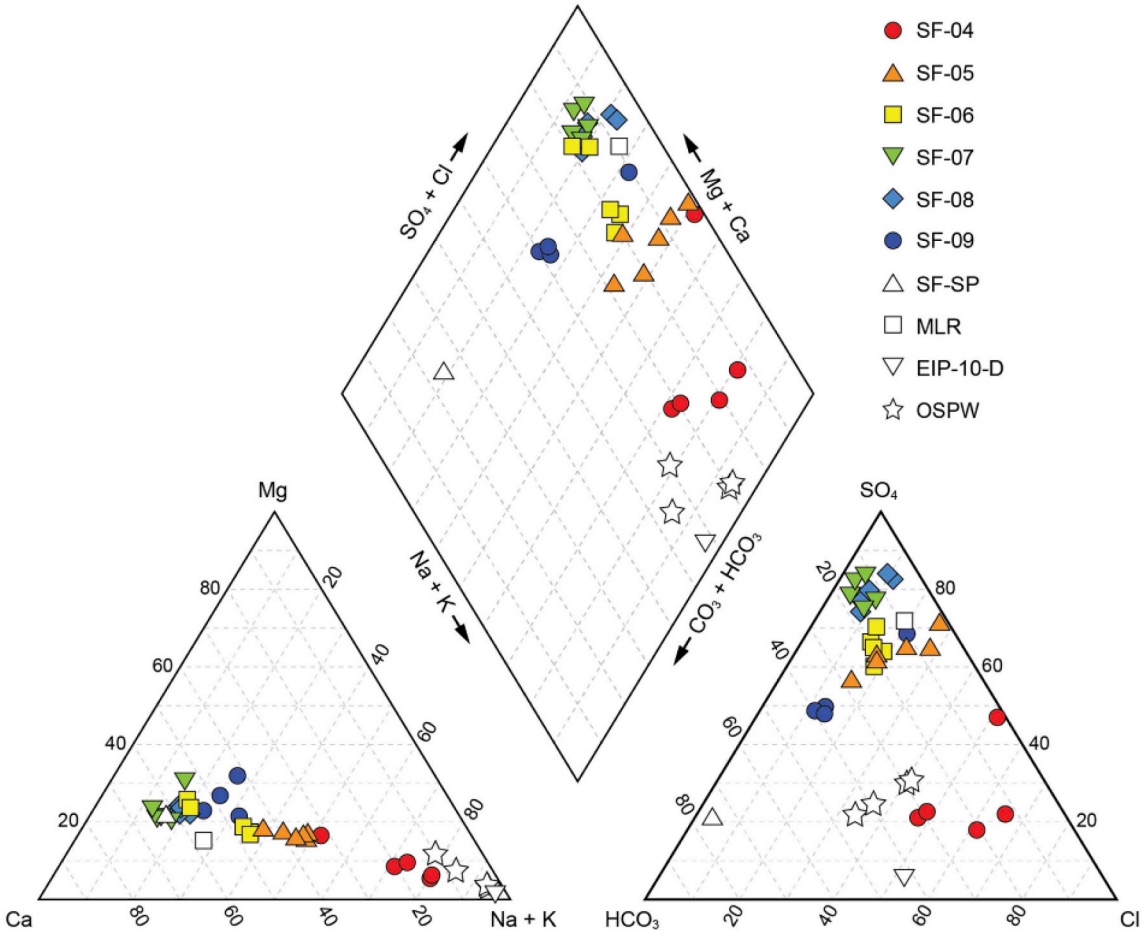

Fig. 3. Piper diagram showing pore water chemistry for soil core samples collected along transect B – B'. Composition of oil sands process-affected water (OSPW) samples from Gibson et al. (2013).

which may be derived from flushing of the tailings sand (Kessel et al., 2018) or CT pore water release. In contrast, the Ca-Mg-SO_4 type water composition is generally consistent with 2012 MLR samples, but not the corresponding SF-SP samples. This trend suggests that soil pore water obtained from location SF-04 was a mixture dominated by OSPW derived from tailings sands and CT, whereas pore water from locations SF-07, SF-08 and SF-09 was a mixture more dominated by MLR water.

To further constrain mixing between OSPW pore water and fresh surface waters along the transect, stable isotopes of water (i.e., $\delta^{18}O$, $\delta^{2}H$) were also measured. Values of $\delta^{18}O$ ranged from −11.23‰ to −18.16‰ while $\delta^{2}H$ values ranged from −107.0‰ to −146.6‰ (Fig. 4). Comparison of these isotopic signatures to data from Baer et al. (2016) on OSPW and natural waters in the region revealed similar signatures to the soil pore water samples. More specifically, samples from locations SF-07 and SF-08 exhibited $\delta^{2}H$ and $\delta^{18}O$ values that fall along the local evaporative line (LEL) but are significantly depleted compared to isotopically enriched OSPW, suggesting these locations are more influenced by local precipitation (Baer et al., 2016). Locations SF-07, SF-08 and SF-09 are also likely influenced by evaporation at the surface resulting in slight isotopic variation at these locations. In contrast, samples for SF-04 and SF-05 exhibited $\delta^{2}H$ and $\delta^{18}O$ values more indicative of evaporation, which is consistent with OSPW from the Mildred Lake Settling Basin and tailings pore waters from Base Mine Lake (Dompierre and Barbour, 2016), which was formerly known as West-In-Pit (Baer et al., 2016). Concomitant increases in Cl concentrations and $\delta^{18}O$ values observed at SF-04, SF-05 and SF-06 are consistent with this interpretation.

The observed spatial trends in pore water composition were consistent with the results from hydrogeological modeling (BGC, 2015). These models predicted a discharge zone at the south margin of the Sandhill Fen wetland area, which aligned with locations where pore water chemistry and isotopic signatures had shifted toward that of OSPW (i.e., SF-04, SF-05, SF-06). The persistence of groundwater with geochemical and isotopic compositions more consistent with MLR (i.e., SF-07, SF-08, SF-09) may be explained by a difference in groundwater sources (i.e. OSPW and meteoric water) at these locations or dilution by fresh surface waters and subsequent flushing.

Depth profiles of pore water chemistry also suggest that capacity for Na attenuation *via* ion exchange was likely limited at location SF-04 and, potentially, declining at locations SF-05 and SF-06. It is assumed, given the relatively uniform distribution of solute concentrations with depth at each location (Fig. 2), that each location represents full equilibration of the profile with some mixture of OSPW and fresh water. The reasons for the composition of the mixture at each location cannot be fully defined; however, they are likely due to some combination of the previously noted upwelling of OSPW over the southern locations combined with the operation of the active water controls within the fen (i.e. flooding with freshwater and operation of the underdrainage system) up to 2014. This apparent absence of Ca or Na attenuation with depth from the pore water sub-samples (Fig. 2), and given that the fen was constructed in 2012, suggests that the Na attenuation within the reclamation soil cover may be short-lived.

3.2. Laboratory column experiments

3.2.1. Column solids

Cation exchange capacity of the till averaged 5.9 ± 0.3 meq $100\,g^{-1}$ (Table S1). The CEC of peat and sand used in these experiments

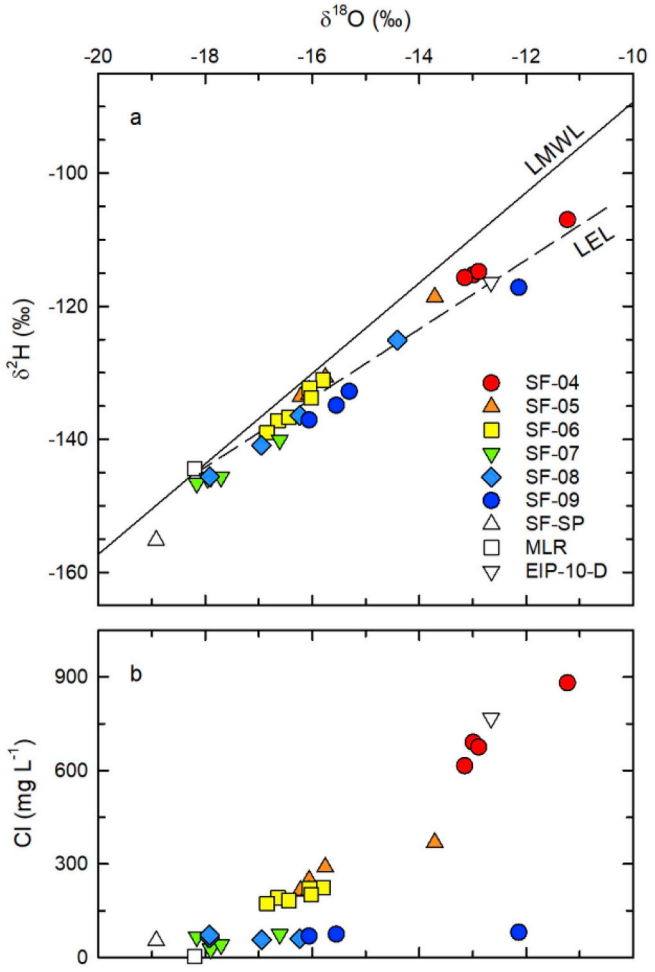

Fig. 4. Plots of (a) δ^2H versus $\delta^{18}O$ and (b) Cl versus $\delta^{18}O$ for pore waters extracted from soil core samples collected along transect B – B′, plus additional water samples from the study site. Solid line on δ^2H versus $\delta^{18}O$ plot denotes weighted local meteoric water line (LMWL) reported by Baer et al. (2016) and dashed line represents the local evaporative line reported by Gibson et al. (2015).

were not quantified; however, previous studies have reported CEC values of 100–500 meq 100 g^{-1} for peat (Clymo, 1983; Kyziol, 2002) and 0.6–2.0 meq 100 g^{-1} for quartz-feldspar sand (Ganguly, 1951; Nash and Marshall, 1956). Porosity was estimated from column volumes, material mass, and particle density. The estimated values for till (0.55), peat (0.80) and sand (0.50) are consistent with values reported by BGC (2015). Approximately 28 mL d^{-1} of input solution was passed through each column over 181 d (Input 1) or 175 d (Input 2), which corresponded to 26, 18, and 29 pore volumes (PVs) for the till, peat, and sand columns, respectively.

3.2.2. Aqueous geochemistry

Input solution pH steadily increased from approximately 8.5 to 9.4 during the experiment. Effluent pH for both till columns (SC-01, SC-02) and both peat columns (SC-03, SC-04) was near-neutral (i.e., 6.9 to 7.1) over the first 14–21 days of the experiment (Fig. 5). Like the input solutions, effluent pH in these columns increased with time and plateaued between 7.7 and 8.1 after approximately 75 days. Effluent pH for both sand columns (SC-05, SC-06) increased during the first 75 days and remained between 8.9 and 9.1 for the remainder of the experiment. Thermodynamic modeling indicated initial effluent pH values were strongly influenced by $CO_{2(g)}$ dissolution associated with column setup. The dissolved CO_2 promoted carbonate dissolution and included ion exchange reactions over the first one to two pore volumes.

Alkalinity was initially elevated within all columns, but decreased over the first 25 days when values were generally consistent with the input solutions. Alkalinity within both till and sand column effluents subsequently mirrored that of the input solution, which averaged 800 mg L^{-1} (as $CaCO_3$). In contrast, alkalinity within the peat columns increased again after 25 d, peaking at approximately 1400 mg L^{-1} (as $CaCO_3$) after 40 d, and declining again to near input values. This alkalinity increase was attributed to microbial oxidation of organic carbon within the peat columns. Observed increases in effluent Fe and Mn concentrations, combined with SO_4 removal, are consistent with this interpretation.

Effluent from the till and peat columns was supersaturated with respect to siderite [$FeCO_3$] and rhodochrosite [$MnCO_3$], suggesting that precipitation of these phases was thermodynamically favorable. Holden et al. (2013) reported similar findings for surficial sediments from the AOSR, where organic carbon ingress associated with OSPW migration induced reductive dissolution of Mn-bearing Fe(III) (hydr)oxides. Corresponding increases in pore water Fe, Mn and HCO_3 concentrations generated conditions favorable to siderite and rhodochrosite precipitation; however, ion exchange may also be an important control on dissolved concentrations of Fe and Mn (Abolfazlzadehdoshanbehbazari et al., 2013; Holden et al., 2013).

Although the sampling frequency was limiting, chloride breakthrough was consistent with advective-dispersive transport at approximately 1 pore volume (PV) and was used as a conservative tracer for reactive transport modeling. Substantial Na attenuation was observed within the till and peat columns (Fig. 6). The effluent Na concentrations from the columns over the first 7 d were approximately one half of the input concentrations (i.e., $C/C_0 = 0.5$). The magnitude of this initial decrease is generally consistent with Na attenuation as reported by Holden et al. (2011) for batch experiments conducted on Pleistocene tills. Nevertheless, effluent Na concentrations for all columns was consistently greater than 500 mg L^{-1}. Sodium attenuation declined over time and, after approximately 75 d, effluent concentrations were greater than 800 mg L^{-1}. Results were generally consistent among columns receiving Input 1 and Input 2, suggesting that the presence of SO_4 had limited impact on Na attenuation. In contrast, Na attenuation within the sand columns (SC-05, SC-06) was limited throughout the experiment.

Effluent Ca concentrations were initially elevated relative to the input solutions, but decreased rapidly over the first 25–75 d of the experiment. Initial effluent Ca concentrations exceeded 1000 mg L^{-1} for the peat columns (SC-03, SC-04) and exceeded 350 mg L^{-1} for the till columns (SC-01, SC-02). Calcium release from the sand columns produced initial effluent concentrations of approximately 350 mg L^{-1} (SC-05) and 140 mg L^{-1} (SC-06). Calcium concentrations decreased rapidly and reached an apparent steady state at approximately 10 and 40 times the input concentrations for till and peat columns, respectively. Thermodynamic modeling indicated that effluent from the till and sand columns was consistently undersaturated with respect to gypsum, whereas initial effluent collected from the peat columns during the first two weeks was supersaturated with respect to gypsum. Similar trends in early effluent concentrations of both Ca and SO_4 from the peat columns suggest that gypsum dissolution likely contributed these ions to solution. A relative increase in effluent EC from the peat columns during this time is also consistent with mineral dissolution. This modeling also indicated that effluent from all columns was consistently supersaturated with respect to calcite [$CaCO_3$] and dolomite [$CaMg(CO_3)_2$], which suggests that carbonate-mineral dissolution was unlikely an important source of dissolved Ca after the first 1 to 2 PVs (~20–30 d).

Magnesium concentrations in column effluents followed similar trends to Ca; however, the magnitude was substantially lower in the till and peat columns (Fig. 6). Early effluent Mg concentrations ranged from 100 to 200 mg L^{-1} for the till columns and from approximately 150 to 300 mg L^{-1} for the peat columns. These concentrations

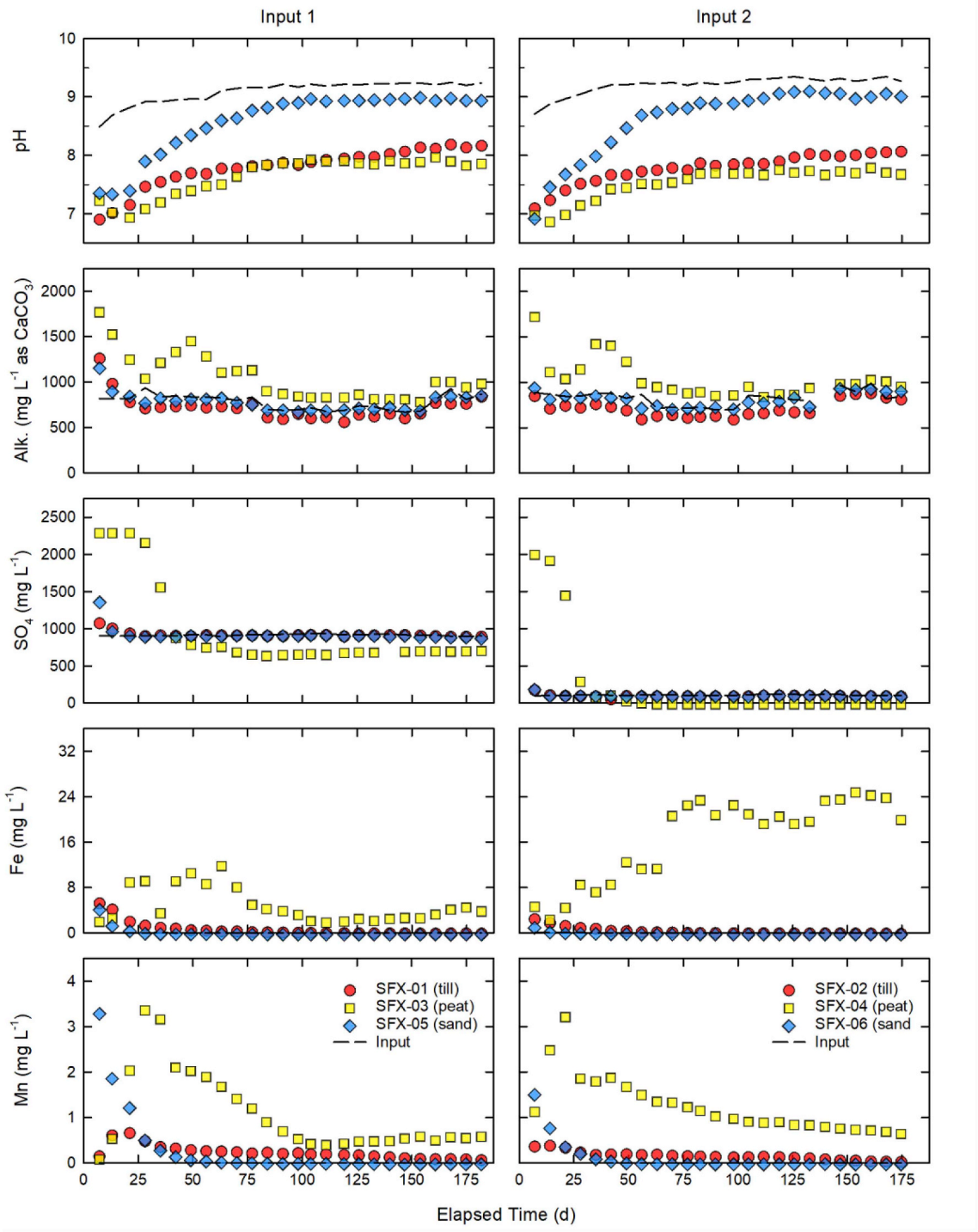

Fig. 5. Input and effluent pH values and alkalinity (Alk.), SO_4, Fe and Mn concentrations over time for till, peat and sand columns receiving input solutions 1 (left column) and 2 (right column).

decreased to near input solution concentrations after 75–100 d for the peat and till columns. In contrast to Ca, this observation suggests that long-term Mg release was limited for these materials. Although effluent Mg concentrations from the sand columns were slightly greater than input concentrations at the first sampling time (7 d), this difference was minimal for the remainder of the experiment.

Potassium transport through the sand columns (SC-05, SC-06) was largely conservative (Fig. 6). Effluent K concentrations for the peat columns were slightly greater than the input solutions over the first 14–21 d, and then slightly less than the input solutions for the remainder of the experiment. Considerable K attenuation was observed over the duration of the experiment for both till columns (i.e., SC-01, SC-02). Similar K results were described by Abolfazlzadehdoshanbehbazari et al. (2013), where K concentrations were consistently lower than that of Na, Ca, and Mg and is therefore likely to be a minor contributor to ion exchange processes.

3.2.3. Mass balance calculations

Mass balance calculations were performed to examine the influence of ion exchange reactions on effluent Na, Ca, Mg and K concentrations.

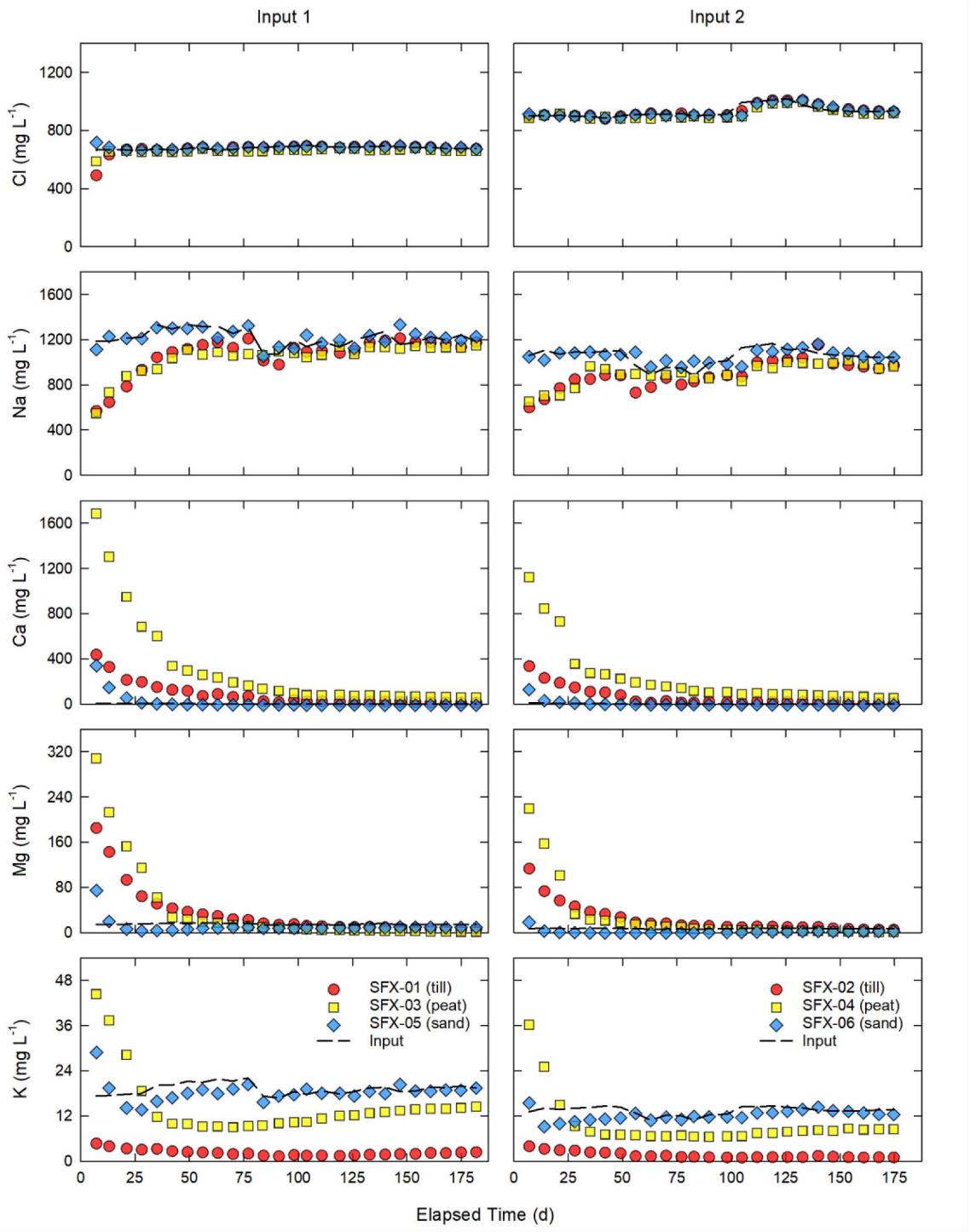

Fig. 6. Input and effluent Na, Ca, Mg and K concentrations over time for till, peat and sand columns receiving Input 1 and Input 2.

The change in mass storage, ΔM_j, for a given solute, j, was calculated by subtracting the cumulative effluent solute mass release, $\sum M_{j_{out}}$, from the input solute mass, $\sum M_{j_{in}}$:

$$\Delta M_j = \sum M_{j_{in}} - \sum M_{j_{out}} \quad (3)$$

where $M_{j_{out}}$ and $M_{j_{in}}$ were calculated as the product of water volume (L), dV_i, over a given sampling interval, i, and the mean concentration (mg L^{-1}) of the solute, $\bar{m}_{j,i}$, over that time interval:

$$M_{j,i} = dV_i\ \bar{m}_{j,i} \quad (4)$$

The cumulative mass, $\sum M_j$, in and out were determined by summing, $M_{j,i}$, over time:

$$\sum M_j = \sum_{i=1}^{n} M_{j,i} \quad (5)$$

For these calculations, positive mass storage values are indicative of solute attenuation, whereas negative values are indicative of solute release.

Cumulative Na mass storage was 0.75–0.93 g for the till and peat columns, which corresponds to between 13 and 16% mass removal over the experiment. However, initial Na mass removal exceeded 50% (Input 1) or 40% (Input 2) for these columns, and steadily declined with time

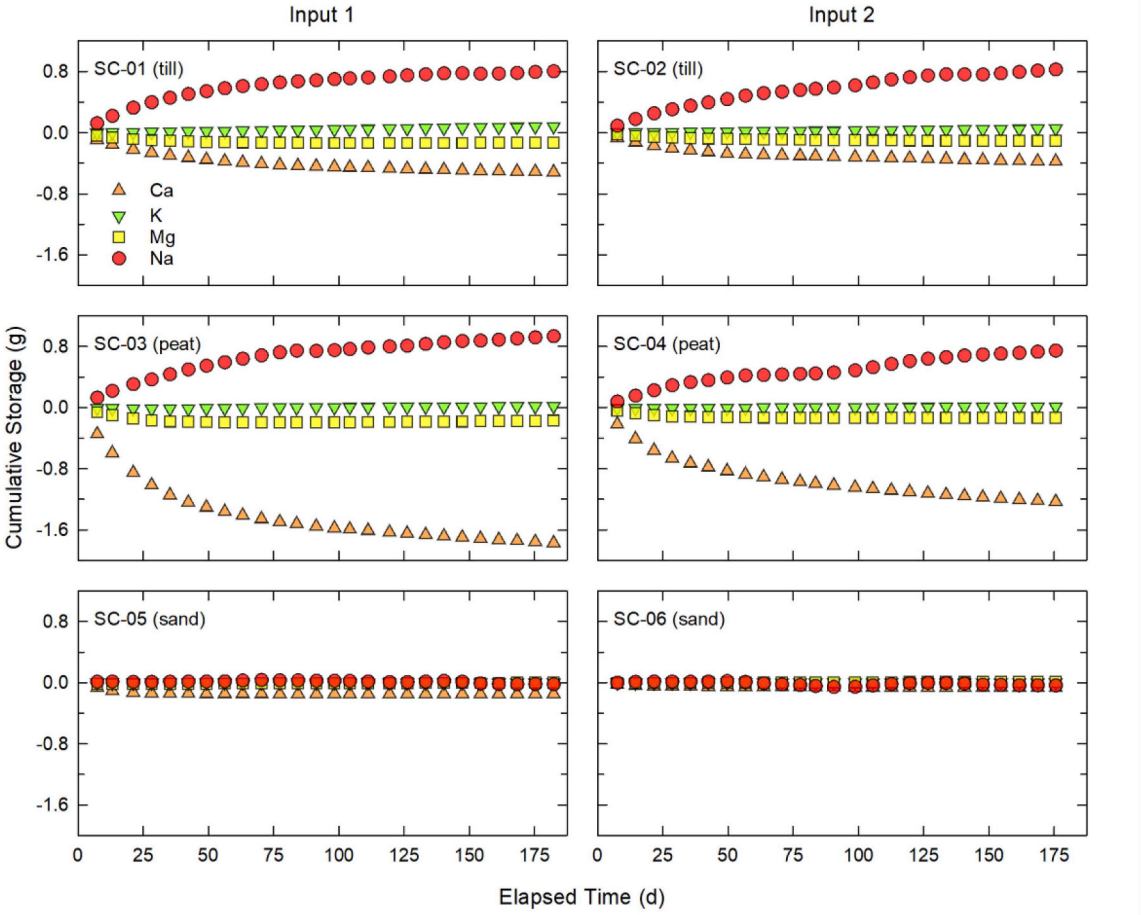

Fig. 7. Cumulative mass storage of sodium (Na), calcium (Ca), magnesium (Mg), and potassium (K) as a function of time.

(Fig. 7). Overall, more than 90% of total Na mass removal in the till and peat columns occurred during the first 7 PV (~40 d) and 4 PV (~50 d) of the experiment, respectively. In contrast to Na, cumulative Ca mass storage was consistently negative with up to 0.52 g and 1.8 g release from the till and peat columns, respectively. These values are consistent with the substantial increases in effluent Ca concentrations relative to the input solutions. Although input SO_4 concentrations did not have a strong influence on Na attenuation, Ca release was greater for columns receiving Input 1 (SC-01, SC-03) compared to Input 2 (SC-02, SC-04). Magnesium mass release (i.e., negative mass storage) ranged from 0.11 to 0.18 g for the till and peat columns, which fits with observed increase in effluent Mg concentrations. Although minor attenuation was observed for all columns, these calculations confirm that K transport was largely conservative. Moreover, these calculations also confirm that mass-transfer reactions had limited influence on effluent Na, Ca, Mg or K concentrations within the sand columns.

3.2.4. Reactive transport modeling

Reactive transport modeling in PHREEQCi (Parkhurst and Appelo, 2013) was used to identify primary biogeochemical reactions controlling the release and attenuation of major ions within reclamation material. The advective-dispersive transport of Cl was modelled initially to constrain the transport parameters (e.g., dispersivity and porosity). Given the limited resolution provided by the sampling frequency it was found that Cl break through could be modelled as equivalent porous media (EPM) advective-dispersive transport.

It is important to note that it is possible that the transport processes may have been affected by preferential flow and the possibility of preferential flow paths cannot be ruled out. If present, preferential flow would facilitate early arrival of solutes and decrease solute (i.e., Na) attenuation (Beven and Germann, 1982). The presence of these types of macroporosity structures have been described for clay rich material (Hendry et al., 1986; Van der Kamp, 1992; Villholth et al., 1998; Cey et al., 2009), as well as peat (Hoag and Price, 1997; Rezanezhad et al., 2012a; Rezanezhad et al., 2016).

Individual columns were equally divided into 10 cells along the model domain, which consisted of 8 cm of reclamation material capped at either end with 1 cm of acid washed silica sand. Measured and simulated physicochemical properties (e.g., CEC) were then distributed accordingly (Table 2). Measured or published CEC data for till, peat and sand were input during model parametrization. Exchange sites (X) were defined for Ca^{2+}, Mg^{2+}, Na^{+} and K^{+}, and the initial composition followed the general order: $CaX_2 > MgX_2 \geq NaX > KX$ (Abolfazlzadehdoshanbehbazari et al., 2013; Holden et al., 2011).

It was found that based on the flow velocities and porosities that the coefficient of hydrodynamic dispersion would be dominated by molecular diffusion. As a result, the longitudinal dispersivity was arbitrarily set to a value of approximately 1/100 of the flow path length (i.e. 0.001 m) Gelhar et al. (1992) and the coefficient of molecular diffusion was set to a value of $4 \times 10^{-10}\,m^2\,s^{-1}$. The Peclet number is much greater than one (ranging from 24 to 35) for the column tests highlighting that the system is defined as an advective-dispersive transport regime.

The initial pore water chemistry was based upon the till pore water composition from field sampling location SF-08. Input 1 and 2 (Table 1) were introduced into the respective columns at a flow rate of 28 mL d^{-1} and model output was observed after reaction in the final cell.

Mass balance calculations indicated that Ca and Mg release was not solely associated with ion exchange reactions. Consequently, solid-

Table 2
Initial physical and geochemical characteristics of columns used for reactive transport modeling.

Parameter	Units	Column ID					
		SF-01	SF-02	SF-03	SF-04	SF-05	SF-06
Material		till	till	peat	peat	sand	sand
Dry Mass	g	600	630	373	358	518	514
Porosity							
total	–	0.55	0.55	0.80	0.80	0.50	0.50
CEC	meq 100 g^{-1}	6.0	6.0	225	225	0.25	0.25
Exchange Sites							
CaX_2	mmol	2.7	2.0	100	100	0.11	0.11
MgX_2	mmol	1.3	1.3	50	50	0.07	0.07
KX	mmol	0.7	0.7	25	25	0.035	0.035
NaX	mmol	1.3	2.0	50	50	0.035	0.035
Reactive Species							
$CaCO_{3(s)}$	mmol	34	37	1166	1119	24	24
$CaMg(CO_3)_{2(s)}$	mmol	17	18	583	559	12	12
$CaSO_4 \cdot 2H_2O_{(s)}$	mmol	0.34	0.36	583	503	0.24	0.24
$CH_2O_{(s)}$	mmol	–	–	10089	9740	–	–
$CO_{2(g)}$	mmol	3.0	3.0	5.0	5.0	1.0	1.0

phase constituents were added to allow for both dissolution and precipitation reactions. Calcite, dolomite and gypsum were included with initial amounts based upon XRD results reported by Holden et al. (2012) and then refined during model calibration. To reflect the initial pore-gas composition prior to water saturation a fixed amount of $CO_{2\ (g)}$ was simulated within each column. Initial carbonate dissolution would have been driven by dissolved $CO_{2\ (g)}$ introduced during column setup, however, this pore water would have been flushed within 1–2 pore volumes. The incorporation of $CO_{2\ (g)}$ and carbonate dissolution in the reactive transport models was reflected in the close fits for pH (Figure S5) and SI; however, discrepancies between modelled and measured pH and SI values are likely due to degassing of $CO_{2\ (g)}$ between sampling periods (Figure S5 and S6). Organic carbon was also included as initial solid-phase components of the peat column to simulate sulfate reduction and $CO_{2\ (g)}$ production. Quality of the reactive transport modeling fits were assessed qualitatively based on fits and supported with RMSE values for major solute constituents, pH and SI for calcite, dolomite, and gypsum (Table S2).

Overall, the models effectively simulated effluent Na, Ca, Mg, K, SO_4

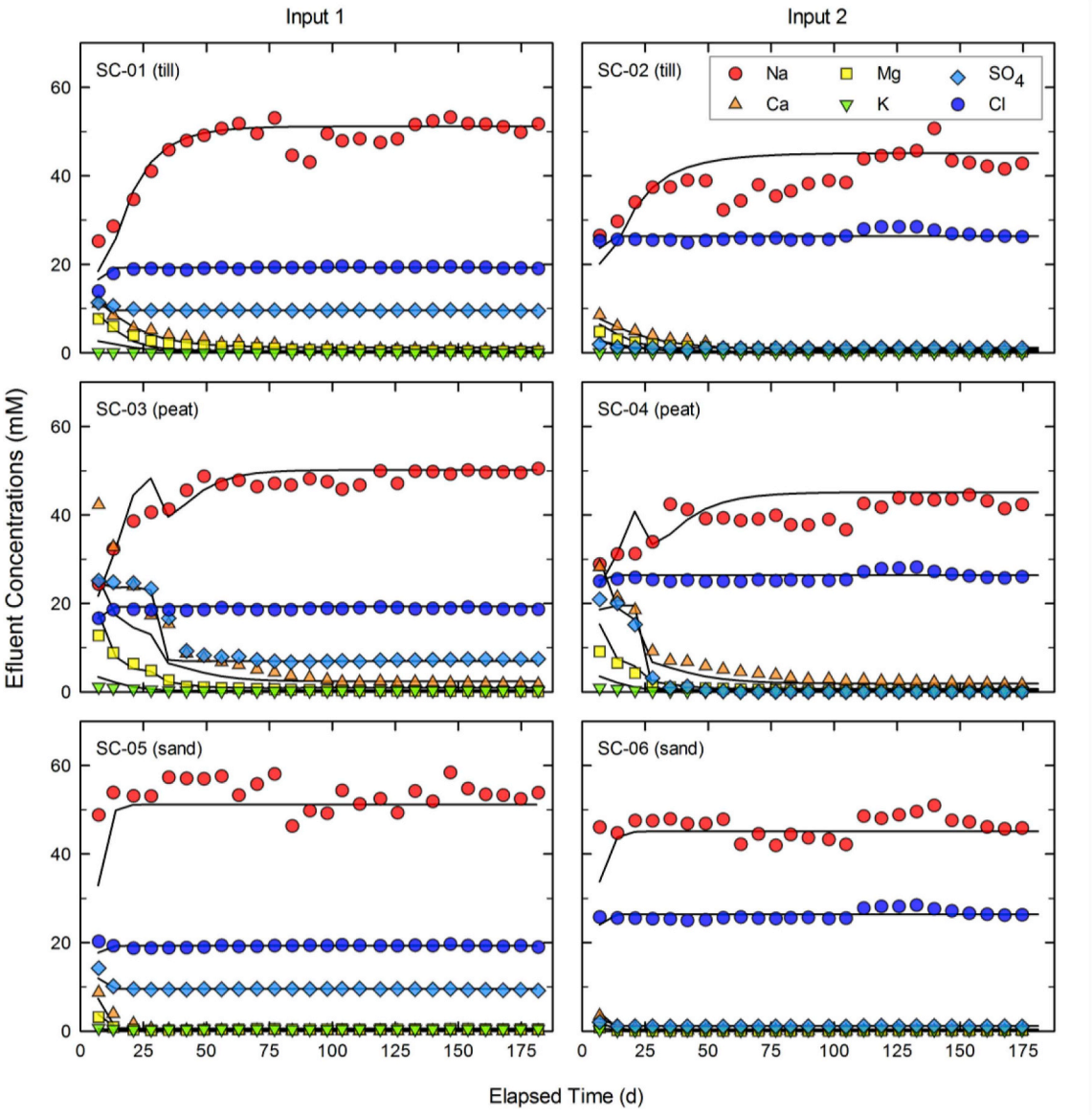

Fig. 8. Measured (symbols) and modelled (lines) effluent Na, Ca, Mg, K, SO_4 and Cl concentrations over time for till, peat and sand columns receiving input solutions 1 (left column) and 2 (right column).

and Cl concentrations for all columns (Fig. 8). Model results confirmed that ion exchange reactions are the dominant mechanism of Na attenuation within till and peat. However, the dissolution of calcite, dolomite and minor amounts of gypsum also influenced Ca and Mg concentrations, which indirectly impacted Na attenuation (Figure S6). Gypsum dissolution at early times was required to simulate early effluent Ca and SO_4 concentrations for all columns. Calcium and SO_4 leaching from peat may also influence effluent concentrations of these constituents (Simhayov et al., 2017). Simulated effluent concentrations were generally consistent with measured data, suggesting that this process had a minor overall influence on effluent Ca and SO_4 concentrations. Effluent pore water from the peat columns (SC-03, SC-04) were brown-yellow in colour suggesting organic complexes may have been a significant source for release of major ions that were not considered in the model. Following initial release, effluent SO_4 concentrations decreased to below input concentrations in the peat columns (SC-03, SC-04). These data were simulated by including the reaction for dissimilatory sulfate reduction:

$$2CH_2O + SO_4^{2-} + H^+ \rightleftharpoons 2CO_2 + HS^- + H_2O \quad (6)$$

Sulfate attenuation has been previously attributed to SO_4 reduction within immobile flow regions during peat column experiments (Rezanezhad et al., 2016).

Column experiments and PHREEQCi modelled outputs demonstrate that reclamation cover systems have a limited capacity to mitigate Na from migrating saline tailings water. Reactive transport modeling assisted in reaffirming the significance of mineralogy, reductive dissolution, biogeochemical processes, and carbonate dissolution-precipitation reactions when considering the fate of saline groundwater or OSPW transport through clay-rich glacial till and peat material.

4. Conclusions

This integrated field, laboratory and modeling study has provided new insight into sodium attenuation processes and capacity within oil sands reclamation soil covers. The field investigation revealed a chemical and isotopic transition in pore water composition along a south-to-north transect of Sandhill Fen. These results indicated that OSPW had migrated through the reclamation soil cover at the southern margin of the wetland area. Minimal evidence of ongoing attenuation in locations where OSPW dominates pore water chemistry suggests that reclamation soil cover materials have a limited and short-lived capacity limit Na transport. This finding was corroborated by the laboratory column experiments, which demonstrated that over 90% of total Na mass removal occurred within the first 4 and 7 pore volumes for the peat and till columns, respectively. Limited Na attenuation by the Pleistocene fluvial sand is consistent with low CEC values for this material. However, maximum decreases in effluent Na concentrations, relative to input values ($\sim$1100 mg L^{-1}), were approximately 40–50% for the first pore volume through the till and peat columns. Consequently, elevated Na concentrations will likely persist, even when attenuation by these soil cover materials is greatest. Reactive transport modeling confirmed interpretations that Na attenuation is controlled by ion exchange reactions with Ca and Mg within till and peat reclamation material. However, Ca and Mg concentrations are directly influenced by mineral precipitation-dissolution reactions and, potentially, leaching from peat. Changes in dissolved Ca and Mg concentrations resulting from these processes can indirectly influence Na attenuation. Overall, this study demonstrates that materials used to construct reclamation soil cover materials have a limited and short-lived capacity for Na attenuation, which should be taken into consideration when designing oil sands mine closure landscapes.

Acknowledgements

Funding was provided to MBJL by the Natural Sciences and Engineering Council of Canada (NSERC) and Syncrude Canada Ltd. through the Industrial Research Chairs program (Grant No. IRCPJ 450684 − 13). Additional support awarded to CVJ through the Brian and Elaine Russel Undergraduate Research Fund and the NSERC Canadian Graduate Scholarships – Master's (NSERC CGS-M) Program. We thank N. Galuschik, C. Cilia, M. Cowell, and Q. Liu for assistance with sample collection and analysis, and J. Essilfie-Dughan for providing input on geochemical modeling. We also thank Dr. Carl Mendoza for providing groundwater chemistry and water table elevation data for wells installed at Sandhill Fen.

Appendix A. Supplementary data

Supplementary data to this article can be found online at https://doi.org/10.1016/j.apgeochem.2018.10.023.

References

Abolfazlzadehdoshanbehbazari, M., Birks, S.J., Moncur, M.C., Ulrich, A.C., 2013. Fate and transport of oil sand process-affected water into the underlying clay till: a field study. J. Contam. Hydrol. 151, 83–92. https://doi.org/10.1016/j.jconhyd.2013.05.002.

Allen, E.W., 2008. Process water treatment in Canada's oil sands industry: I. Target pollutants and treatment objectives. J. Environ. Eng. Sci. 7, 123–138. https://doi.org/10.1139/S07-038.

Apostol, K.G., Zwiazek, J.J., MacKinnon, M.D., 2004. Naphthenic acids affect plant water conductance but do not alter shoot Na^+ and Cl^- concentrations in jack pine (Pinus banksiana) seedlings. Plant Soil 263 (1), 183–190. https://doi.org/10.1023/B:PLSO.0000047725.04930.bc.

Ball, J.W., Nordstrom, D.K., 1991. User's manual for WATEQ4F, with revised thermodynamic database and test cases for calculating speciation of major. In: Trace and Redox Elements in Natural Water: U.S. Geological Survey, Open-file Report, pp. 91–183.

Baer, T., Barbour, S.L., Gibson, J.J., 2016. The stable isotopes of site wide waters at an oil sands mine in northern Alberta, Canada. J. Hydrol. 541, 1155–1164. https://doi.org/10.1016/j.jhydrol.2016.08.017.

BGC Engineering Inc, 2015. Sandhill Fen: Numerical Groundwater Modelling, Project No. 0534135. Submitted to Syncrude Canada Ltd., June 12, 2015.

Beven, K., Germann, P., 1982. Macropores and water flow in soils. Water Resour. Res. 18, 1311–1325. https://doi.org/10.1029/WR018i005p01311.

Bradford, L.M., Ziolkowski, L.A., Goad, C., Warren, L.A., Slater, G.F., 2017. Elucidating carbon sources driving microbial metabolism during oil sands reclamation. J. Environ. Manag. 188, 246–254. https://doi.org/10.1016/j.jenvman.2016.11.029.

Carroll, D., 1959. Ion exchange in clays and other minerals. Geol. Soc. Am. Bull. 70, 749–779. https://doi.org/10.1130/0016-7606(1959)70[749:IEICAO]2.0.CO;2.

Chalaturnyk, R.J., Scott, J.D., Özüm, B., 2002. Management of oil sands tailings. Petrol. Sci. Technol. 20 (9–10), 1025–1046. https://doi.org/10.1081/LFT-120003695.

Cey, E.E., Rudolph, D.L., Passmore, J., 2009. Influence of macroporosity on preferential solute and colloid transport in unsaturated field soils. J. Contam. Hydrol. 107 (1–2), 45–57. https://doi.org/10.1016/j.jconhyd.2009.03.004.

Cilia, C.R.C., 2017. Characterizing the Physical and Chemical Transport of Dissolved Salts in Layered Oil Sands Mine Wastes Undergoing Reclamation. M.Sc. Thesis, University of Saskatchewan, Saskatoon, Canada 150 pp.

Clymo, R.S., 1983. Peat. In: Gore, A.J.P. (Ed.), Ecosystems of the World 4a: Mires: Swamp, Bog, Fen and Moor. Elsevier Scientific Publishing Company, New York, pp. 159–224.

Curtin, D., Naidu, R., 1998. Fertility constraints to plant production. In: Sumner, M.E., Naidu, R. (Eds.), In Sodic Soil: Distribution, Management and Environmental Consequences. Oxford University Press, New York, pp. 107–123.

Dompierre, K.A., Lindsay, M.B.J., Cruz-Hernández, P., Halferdahl, G.M., 2016. Initial geochemical characteristics of fluid fine tailings in an oil sands end pit lake. Sci. Total Environ. 556, 196–206. https://doi.org/10.1016/j.scitotenv.2016.03.002.

Dompierre, K.A., Barbour, S.L., 2016. Characterization of physical mass transport through oil sands fluid fine tailings in an end pit lake: a multi-tracer study. J. Contam. Hydrol. 189, 12–26. https://doi.org/10.1016/j.jconhyd.2016.03.006.

Ferone, J.M., Devito, K.J., 2004. Shallow groundwater–surface water interactions in pond–peatland complexes along a Boreal Plains topographic gradient. J. Hydrol. 292 (1–4), 75–95. https://doi.org/10.1016/j.jhydrol.2003.12.032.

Ganguly, A.K., 1951. Base-exchange capacity of silica and silicate minerals. J. Phys. Colloid Chem. 55, 1417–1428. https://doi.org/10.1021/j150492a002.

Gelhar, L., Welty, C., Rehfeld, K.R., 1992. A critical review of data on field-scale dispersion in aquifers. Water Resour. Res. 28, 1955–1974. https://doi.org/10.1029/92WR00607.

Gibson, J.J., Fennell, J., Birks, S.J., Yi, Y., Moncur, M.C., Hansen, B., Jasechko, S., 2013. Evidence of discharging saline formation water to the Athabasca River in the oil sands mining region, northern Alberta. Can. J. Earth Sci. 50, 1244–1257. https://doi.org/10.1139/cjes-2013-0027.

Gibson, J.J., Birks, S.J., Vitt, D.H., 2015. Runoff to boreal lakes linked to land cover, watershed morphology and permafrost thaw: a 9-year isotope mass balance assessment. Hydrol. Process. 29, 3848–3861. https://doi.org/10.1002/hyp.10502.

Glaeser, L.C., Vitt, D.H., Ebbs, S., 2016. Responses of the wetland grass, *Beckmannia syzigachne*, to salinity and soil wetness: consequences for wetland reclamation in the oil sands area of Alberta, Canada. Ecol. Eng. 86, 24–30. https://doi.org/10.1016/j.ecoleng.2015.10.009.

Gosselin, P., Hrudey, S.E., Naeth, M.A., Plourde, A., Therrien, R., Van Der Kraak, G., Xu, Z., 2010. Environmental and Health Impacts of Canada's Oils Sands Industry. The Royal Society of Canada, Ottawa, Canada, pp. 440.

Government of Alberta, 2017. Regional reclamation and disturbance tracking by year. In: Oil Sands Information Portal. Alberta Environment and Parks Data Library. http://osip.alberta.ca/library/Dataset/Details/27, Accessed date: 24 April 2018.

Gražulis, S., Chateigner, D., Downs, R.T., Yokochi, A.F.T., Quirós, M., Lutterotti, L., Manakova, E., Butkus, J., Moeck, P., Le Bail, A., 2009. Crystallography open database - an open-access collection of crystal structures. J. Appl. Crystallogr. 42, 726–729. https://doi.org/10.1107/S0021889809016690.

Hendry, M.J., Cherry, J.A., Wallick, E.I., 1986. Origin and distribution of sulfate in a fractured till in southern Alberta, Canada. Water Resour. Res. 22, 45–61. https://doi.org/10.1029/WR022i001p00045.

Hoag, R.S., Price, J.S., 1997. The effects of matrix diffusion on solute transport and retardation in undisturbed peat in laboratory columns. J. Contam. Hydrol. 28, 193–205. https://doi.org/10.1016/S0169-7722(96)00085-X.

Holden, A.A., Donahue, R.B., Ulrich, A.C., 2011. Geochemical interactions between process-affected water from oil sands tailings ponds and North Alberta surficial sediments. J. Contam. Hydrol. 119, 55–68. https://doi.org/10.1016/j.jconhyd.2010.09.008.

Holden, A.A., Mayer, K.U., Ulrich, A.C., 2012. Evaluating methods for quantifying cation exchange in mildly calcareous sediments in Northern Alberta. Appl. Geochem. 27, 2511–2523. https://doi.org/10.1016/j.apgeochem.2012.08.026.

Holden, A.A., Haque, S.E., Mayer, K.U., Ulrich, A.C., 2013. Biogeochemical processes controlling the mobility of major ions and trace metals in aquitard sediments beneath an oil sand tailing pond: laboratory studies and reactive transport modeling. J. Contam. Hydrol. 151, 55–67. https://doi.org/10.1016/j.jconhyd.2013.04.006.

Kasperski, K.L., Mikula, R.J., 2011. Waste streams of mined oil sands: characteristics and remediation. Elements 7, 387–392. https://doi.org/10.2113/gselements.7.6.387.

Ketcheson, S.J., Price, J.S., Sutton, O., Sutherland, G., Kessel, E., Petrone, R.M., 2017. The hydrological functioning of a constructed fen wetland watershed. Sci. Total Environ. 603–604, 593–605. https://doi.org/10.1016/j.scitotenv.2017.06.101.

Ketcheson, S.J., Price, J.S., Carey, S.K., Petrone, R.M., Mendoza, C.A., Devito, K.J., 2016. Constructing fen peatlands in post-mining oil sands landscapes: challenges and opportunities from a hydrological perspective. Earth Sci. Rev. 161, 130–139. https://doi.org/10.1016/j.earscirev.2016.08.007.

Kessel, E.D., Ketcheson, S.J., Price, J.S., 2018. The distribution and migration of sodium from a reclaimed upland to a constructed fen peatland in a post-mined oil sands landscape. Sci. Total Environ. 630, 1553–1564. https://doi.org/10.1016/j.scitotenv.2018.02.253.

Kessler, S., Barbour, S.L., Van Rees, K.C., Dobchuk, B.S., 2010. Salinization of soil over saline-sodic overburden from the oil sands in Alberta. Can. J. Soil Sci. 90 (4), 637–647. https://doi.org/10.4141/cjss10019.

Kyziol, J., 2002. Effect of physical properties and cation exchange capacity on sorption of heavy metals onto peat. Pol. J. Environ. Stud. 11 (6), 713–718.

MacKinnon, M.D., Matthews, J.G., Shaw, W.H., Cuddy, R.G., 2001. Water quality issues associated with composite tailings (CT) technology for managing oil sands tailings. Int. J. Surf. Min. Reclamat. Environ. 15, 235–256. https://doi.org/10.1076/ijsm.15.4.235.7416.

Matthews, J.G., Shaw, W.H., MacKinnon, M.D., Cuddy, R.G., 2002. Development of composite tailings technology at Syncrude. Int. J. Surf. Min. Reclamat. Environ. 16, 24–39. https://doi.org/10.1076/ijsm.16.1.24.3407.

McCarter, C.P.R., Weber, T.K.D., Price, J.S., 2018. Competitive transport processes of chloride, sodium, potassium, and ammonium in fen peat. J. Contam. Hydrol. https://doi.org/10.1016/j.jconhyd.2018.08.004. (in press).

Moncur, M.C., Blowes, D.W., Ptacek, C.J., 2013. Pore water extraction from the unsaturated and saturated zones. Can. J. Earth Sci. 50, 1051–1058. https://doi.org/10.1139/cjes-2012-0165.

Moore, D.M., Reynolds, R.C., 1999. X-Ray Diffraction and the Identification and Analysis of Clay Minerals, second ed. Oxford University Press, New York 400 pp.

Nash, V.E., Marshall, C.E., 1956. The surface reactions of silicate minerals. II. Reactions of feldspar surfaces with salt solutions. University of Missouri, College of Agriculture, Agricultural Experiment Station. Res. Bull. 614 36pp.

Nicholls, E.M., Carey, S.K., Humphreys, E.R., Clark, M.G., Drewitt, G.B., 2016. Multi-year water balance assessment of a newly constructed wetland, Fort McMurray, Alberta. Hydrol. Process. 30, 2739–2753. https://doi.org/10.1002/hyp.10881.

NorthWind Land Resources, Inc, 2014. 2013 Sandhill Fen Soil Sampling Program. Technical Report, Project #13-328, Edmonton, Canada. 55 pp.

Oswald, C.J., Carey, S.K., 2016. Total and methyl mercury concentrations in sediment and water of a constructed wetland in the Athabasca Oil Sands Region. Environ. Pollut. 213, 628–637. https://doi.org/10.1016/j.envpol.2016.03.002.

Parkhurst, D.L., Appelo, C.A.J., 2013. Description of input and examples for PHREEQC version 3—a computer program for speciation, batch-reaction, one-dimensional transport, and inverse geochemical calculations. In: Techniques and Methods 6-A43. U.S. Geological Survey, Denver, USA 497 pp.

Price, J.S., McLaren, R.G., Rudolph, D.L., 2010. Landscape restoration after oil sands mining: conceptual design and hydrological modelling for fen reconstruction. Int. J. Min. Reclamat. Environ. 24, 109–123. https://doi.org/10.1080/17480930902955724.

Pouliot, R., Rochefort, L., Graf, M.D., 2012. Impacts of oil sands process water on fen plants: implications for plant selection in required reclamation projects. Environ. Pollut. 167, 132–137. https://doi.org/10.1016/j.envpol.2012.03.050.

Qadir, M., Schubert, S., 2002. Degradation processes and nutrient constraints in sodic soils. Land Degrad. Dev. 13, 275–294. https://doi.org/10.1002/ldr.504.

Reid, M.L., Warren, L.A., 2016. S reactivity of an oil sands composite tailings deposit undergoing reclamation wetland construction. J. Environ. Manag. 166, 321–329. https://doi.org/10.1016/j.jenvman.2015.10.014.

Rengasamy, P., Sumner, M.E., 1998. Processes involved on sodic behaviour. In: Sumner, M.E., Naidu, R. (Eds.), Sodic Soil: Distribution, Management and Environmental Consequences. Oxford University Press, New York, pp. 35–50.

Rezanezhad, R., Price, J.S., Craig, J.R., 2012a. The effects of dual porosity on transport and retardation in peat: a laboratory experiment. Can. J. Soil Sci. 92, 723–732. https://doi.org/10.4141/cjss2011-050.

Rezanezhad, F., Andersen, R., Pouliot, R., Price, J.S., Rochefort, L., Graf, M.D., 2012b. How fen vegetation structure affects the transport of oil sands process-affected waters. Wetlands 32, 557–570. https://doi.org/10.1007/s13157-012-0290-z.

Rezanezhad, F., Price, J.S., Quinton, W.L., Lennartz, B., Milojevic, T., Van, C., 2016. Structure of peat soils and implications for water storage, flow and solute transport: a review update for geochemists. Chem. Geol. 429, 75–84. https://doi.org/10.1016/j.chemgeo.2016.03.010.

Scarlett, S.J., Petrone, R.M., Price, J.S., 2017. Controls on plot-scale evapotranspiration from a constructed fen in the Athabasca oil sands region, Alberta. Ecol. Eng. 100, 199–210. https://doi.org/10.1016/j.ecoleng.2016.12.020.

Simhayov, R.B., Price, J.S., Smeaton, C.M., Parsons, C., Rezanezhad, F., Van Cappellen, P., 2017. Solute pools in Nikanotee Fen watershed in the Athabasca oil sands region. Environ. Pollut. 225, 150–162. https://doi.org/10.1016/j.envpol.2017.03.038.

Suarez, D.L., Rhoades, J.D., Savado, R., Grieve, C.M., 1984. Effect of pH on saturated hydraulic conductivity and soil dispersion. Soil Sci. Soc. Am. J. 48, 50–55. https://doi.org/10.1080/00103629609369702.

Van der Kamp, G., 1992. Evaluating the effects of fractures on solute transport through fractured clayey aquitards. In: Proceedings of 1992 Conference of International Association of Hydrogeologists.

Villholth, K.G., Jensen, K.H., Fredericia, J., 1998. Flow and transport processes in a macroporous subsurface-drained glacial till soil I: field investigations. J. Hydrol. 207, 98–120. https://doi.org/10.1016/S0022-1694(98)00129-2.

Vitt, D.H., House, M., Hartsock, J.A., 2016. Sandhill Fen, an initial trial for wetland species assembly on in-pit substrates: lessons after three years. Botany 94, 1015–1025. https://doi.org/10.1139/cjb-2015-0262.

Vitt, D., Halsey, L., Thormann, M., Martin, T., 1996. Peatland Inventory of Alberta. Phase 1: Overview of Peatland Resources in the Natural Regions and Subregions of the Province. University of Alberta, Edmonton.

Wassenaar, L.I., Hendry, M.J., Chostner, V.L., Lis, G.P., 2008. High resolution pore water δ^2H and $\delta^{18}O$ measurements by $H_2O_{(liquid)}$-$H_2O_{(vapor)}$ equilibration laser spectroscopy. Environ. Sci. Technol. 42, 9262–9267. https://doi.org/10.1021/es802065s.